

Atmospheric feedbacks on Arctic summer sea-ice anomalies in ensemble simulations of a coupled regional climate model

Annette RINKE^{1*}, Dörthe HANDORF¹, Wolfgang DORN¹, Klaus DETHLOFF¹, John C. MOORE² & Xiangdong ZHANG³

¹ Alfred Wegener Institute, Helmholtz Centre for Polar and Marine Research, Potsdam 14473, Germany;

² College of Global Change and Earth System Science, Beijing Normal University, Beijing 100875, China;

³ International Arctic Research Center, University of Alaska Fairbanks, Alaska 99775, USA

Received 18 May 2018; accepted 13 August 2018

Abstract Ensemble simulations with the Arctic coupled regional climate model HIRHAM-NAOSIM have been analyzed to investigate atmospheric feedbacks to September sea-ice anomalies in the Arctic in autumn and the following winter. Different “low minus high ice” composites have been calculated using selected model runs and different periods. This approach allows us to investigate the robustness of the simulated regional atmospheric feedbacks to detected sea-ice anomalies. Since the position and strength of the September sea-ice anomaly varies between the different “low minus high ice” composites, the related simulated atmospheric patterns in autumn differ depending on the specific surface heat flux forcing through the ocean-atmosphere interface. However, irrespective of those autumn differences, the regional atmospheric feedback in the following winter is rather insensitive to the applied compositing. Neither the selection of simulations nor the considered period impacts the results. The simulated consistent large-scale atmospheric circulation pattern shows a wave-like pattern with positive pressure anomaly over the region of the Barents/Kara Seas and Scandinavia/western Russia (“Scandinavian-Ural blocking”) and negative pressure anomaly over the East Siberian/Laptev Seas.

Keywords Arctic climate, atmosphere-sea ice feedback, regional climate modeling, Arctic atmosphere

Citation: Rinke A, Handorf D, Dorn W, et al. Atmospheric feedbacks on Arctic summer sea-ice anomalies in ensemble simulations of a coupled regional climate model. *Adv Polar Sci*, 2018, 29(3): 156-164, doi: 10.13679/j.advps.2018.3.00156

1 Introduction

Arctic climate changes appear faster than in other regions of the world, recognizable by the so-called ‘Arctic amplification’, but individual feedback mechanisms and their contribution are still under debate (see the overview by Wendisch et al., 2017; Cohen et al., 2014; Serreze and Barry, 2011). One of the major characteristics of the ‘new Arctic’ (Jeffries et al., 2013) is the rapidly declining Arctic sea ice

particularly in late summer (see the overview by Stroeve et al., 2012). Associated with reduced sea-ice cover are increased heat and moisture fluxes into the atmosphere, near-surface warming and reduced static atmospheric stability, which can, in turn, further affect changes in the atmospheric circulation (see overview of Vihma, 2014). However, we still need a better understanding of how the atmosphere may respond to Arctic sea-ice reductions. Research questions include those of consistency and thus robustness of results considering different observational and model data sets and periods (e.g., Semenov and Latif, 2015). Still, the imprint of late summer sea-ice anomalies on the following winter

* Corresponding author, E-mail: Annette.Rinke@awi.de

atmospheric circulation is under debate. Many studies on linkages of Arctic sea-ice reduction and atmospheric circulation have applied atmosphere-only models (e.g., Screen, 2017; Jaiser et al., 2016; Peings and Magnusdottir, 2014; Screen et al., 2013; Porter et al., 2012). Those studies lack potentially important atmosphere-ice-ocean feedbacks.

Our study applies a fully coupled atmosphere-ice-ocean regional climate model (RCM) over the Arctic, called HIRHAM-NAOSIM. A detailed model description is given by Dorn et al. (2009). The RCM approach allows ‘realistic’ large-scale lateral atmospheric forcing from reanalyses. The model has an improved description of Arctic regional processes and reproduces observed atmosphere-sea ice relationships (Rinke et al., 2013; Dorn et al., 2012). In a previous study, we described the simulated regional atmospheric feedbacks associated with late summer sea-ice anomalies based on six-member ensemble simulations over the period 1949–2008 (Rinke et al., 2013). Here we extend this study and analyze a larger set of ensemble simulations from this coupled Arctic RCM by including a 10-member ensemble simulation over 1979–2014. The aim is to explore the robustness and, accordingly, the uncertainty of the simulated atmospheric response to September sea-ice anomalies by analyzing different simulations and different periods.

2 Simulations and composites

2.1 Ensemble simulations

Two sets of ensemble simulations are analyzed here, which differ by their atmospheric lateral boundary forcing.

The first set is based on HIRHAM-NAOSIM simulations, laterally driven by National Centers for Environmental Prediction (NCEP)/National Center for Atmospheric Research (NCAR) reanalysis (Kalnay et al., 1996) for the 60-year period of 1949–2008. All ensemble members were started equally on 1 January 1948 and run through 31 December 2008, but the initial ice-ocean fields were taken from different years of a preceding coupled spin-up. The ensemble consists of six members, which were started with the ice-ocean states of 1 January of six different years (1955, 1956, 1957, 1958, 1959, 1960) from the spin-up run. Details on the setup of these runs can be found in Dorn et al. (2012). In the following, we call these runs “NCEP-driven runs”.

The second set is based on HIRHAM-NAOSIM simulations, laterally driven by the European Centre for Medium-Range Weather Forecasts (ECMWF) Interim reanalysis (ERA-Interim; Dee et al., 2011) for the 36-year period of 1979–2014. All ensemble members were started equally on 1 January 1979 and run through 31 December 2014, but the initial ice-ocean fields were taken from different years of the above described NCEP-driven runs. This ensemble includes 10 members. Five runs were started with the ice-ocean state from the NCEP-driven run #1,

while the other five were started with those from the NCEP-driven run #6. In either case, these runs were initialized with the ice-ocean states of 1 January of the five different years (1975, 1976, 1977, 1978, 1979) from the respective NCEP-run. In the following, we call these runs “ERA-driven runs”.

2.2 Composite analysis

We follow Rinke et al. (2013) for the calculation of composites of low- and high-ice years, based on the September Arctic sea-ice area anomaly. As we are interested in the robustness of the atmospheric patterns in response to different magnitudes of sea-ice anomalies, various composites with respect to different time periods have been computed (Figure 1). We consider the following four different sets of composites: From the NCEP-driven runs, low- and high-ice composites have been calculated for two periods. On the one hand, composites have been determined based on the whole time period 1949–2008, for which the sea ice area anomalies have been calculated relative to the 1961–1990 mean. These results are based on Rinke et al. (2013). On the other hand, composites have been calculated based on the overlapping period (1979–2008) with the ERA-driven run. For this, the sea-ice anomalies have been calculated with respect to the 1979–2008 mean. Analogously, 1979–2008 composites have been calculated from the ERA-driven runs. In addition, sea-ice anomalies

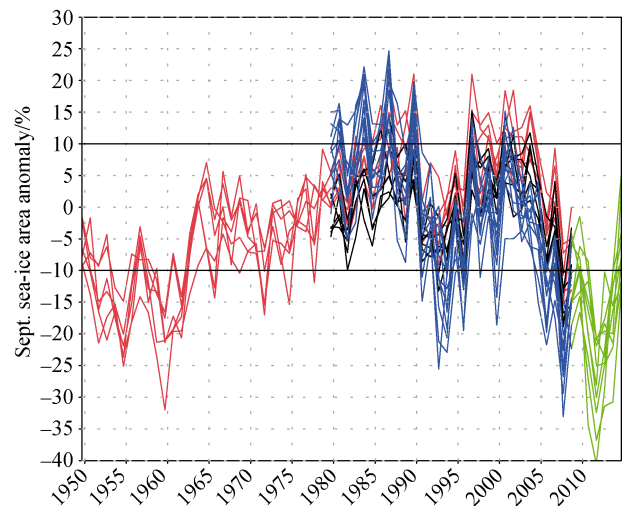


Figure 1 Simulated Arctic September sea-ice area anomalies (%). Different colors show the anomalies for different runs (NCEP- or ERA-driven) and different periods: NCEP-driven run 1949–2008 relative to 1961–1990 (red), NCEP-driven run 1979–2008 relative to 1979–2008 (black), ERA-driven run 1979–2008 relative to 1979–2008 (blue), ERA-driven run 1979–2014 relative to 1979–2008 (green). The lines represent the individual ensemble members. Analyzed low- and high-ice years are those with anomalies larger than -10% and $+10\%$, respectively. The anomalies always refer to the average in the respective ensemble member.

for the whole integration period 1979–2014 have been calculated from the ERA-driven runs, again relative to the 1979–2008 mean.

In general, the September sea-ice area anomalies have been calculated from the simulated sea-ice concentration for each year of the respective time series and for each of the ensemble members. Based on these sea-ice area anomalies, low- and high-ice years have been selected for each ensemble member and assembled to composite means. Low- and high-ice years have been selected when the deviation to the mean of the reference period is larger than 10% (Figure 1). This 10% threshold is approximately equivalent to a one-standard-deviation anomaly.

Figure 2 shows the associated simulated “low minus high ice” sea-ice concentration differences. In autumn, prominent sea-ice reduction occurs in the northern Barents, Kara, Laptev, East Siberian, Chukchi, and Beaufort Seas, while in winter the sea-ice reduction is limited to the

Barents Sea. In general, the maximum across-ensemble variance of the sea-ice concentration anomaly emerges in the region where the maximum of the ensemble mean sea-ice concentration anomaly occurs. This indicates that the individual ensemble members largely agree on the location of the sea-ice anomaly, but its strength varies. Comparing the different ensembles, specific differences become obvious. In autumn, the sea-ice anomalies in the NCEP-driven runs are stronger over the northern Barents/Kara Seas as compared to the ERA-driven runs. In contrast, the ERA-driven runs show a stronger sea-ice anomaly in the East Siberian/Chukchi Seas. In winter, the sea-ice concentration anomaly in the Barents Sea is clearly stronger (almost doubled) in the NCEP-driven runs. Interestingly, for given runs, the period chosen for the low- and high-ice composites shows less impact on the sea-ice anomaly than between the NCEP- and ERA-driven runs.

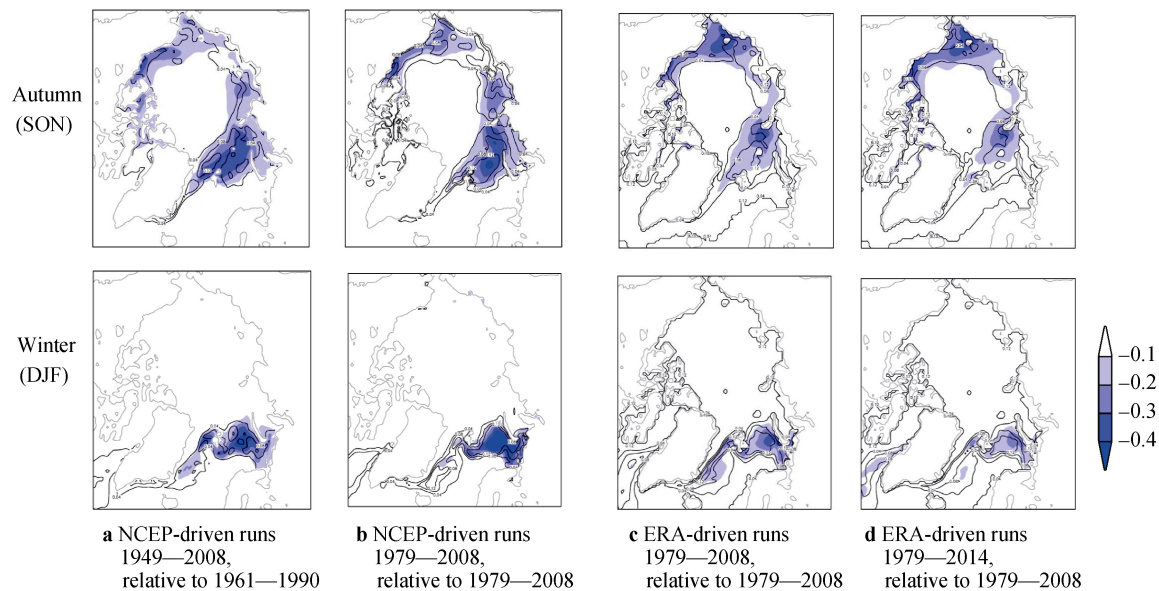


Figure 2 Simulated sea-ice concentration difference “low minus high ice” for autumn (upper panel) and the following winter (lower panel), averaged over the respective ensemble members (color shading). The isolines show the across-ensemble standard deviation of the sea-ice concentration difference. The different plots show the results for different runs (NCEP- or ERA-driven) and different periods (as given in Figure 1).

3 Atmospheric feedbacks

To analyze atmospheric feedbacks associated with the sea-ice anomalies, composites of atmospheric variables for the selected low- and high-ice cases have been calculated for each of the ensemble members. Seasonal differences “low minus high ice” for autumn (September–November; SON) and the following winter (December–February; DJF) are discussed in this section. We focus on the following atmospheric variables: The surface turbulent heat flux and surface air temperature (SAT) characterize the near-surface thermodynamic effects, while the mean sea level pressure (SLP) describes the near-surface dynamical effect. Further,

we use the geopotential thickness (defined as the difference between the 500 hPa and 850 hPa geopotential heights; z_{500} – z_{850}) and the 500 hPa geopotential height (z_{500}) to analyze the effects in the free troposphere.

3.1 Autumn

The autumn surface sensible and latent heat fluxes and surface air temperature differs in the different “low minus high ice” composites (Figures 3 and 4), corresponding to the different sea-ice concentration anomalies (Figure 2). However, consistently, the total turbulent heat flux anomalies are in the range between $-10 \text{ W}\cdot\text{m}^{-2}$ and $-20 \text{ W}\cdot\text{m}^{-2}$, and can reach up to $-40 \text{ W}\cdot\text{m}^{-2}$. The maximum heat flux anomalies

occur generally over the northern Barents/Kara Seas, and the Beaufort, Chukchi, East Siberian and Laptev Seas. However, their specific local amplitude differs among the four composites. The associated increase in SAT is up to *ca.* 6 K, distinctively captured over the regions of the sea-ice anomaly, but differs across the composites, which can be attributed to difference in the turbulent heat fluxes and associated changes in the atmospheric circulation as discussed below. The free troposphere shows a warm anomaly over most parts of the Arctic Ocean, manifested by an increase in the 850–500-hPa layer thickness. However, the strength differs considerably and the spatial pattern of the free-tropospheric warming

follows the 850-hPa warming pattern (Rinke et al., 2006) and is related to the near-surface warming (positive/negative thickness anomalies are associated with positive/negative SAT anomalies). While the maximum free-tropospheric thickening of up to 15 m is centered over the Barents/Kara Seas in the NCEP-driven runs composite from the long period, there are different anomalies in the other three composites. There, the maximum free-tropospheric warming is shifted towards lower latitudes, and negative anomalies occur over Russian coastal lands (ERA-driven runs) and over the region of Canadian Archipelago-Baffin Bay-Greenland-Fram Strait (shorter period NCEP-driven runs).

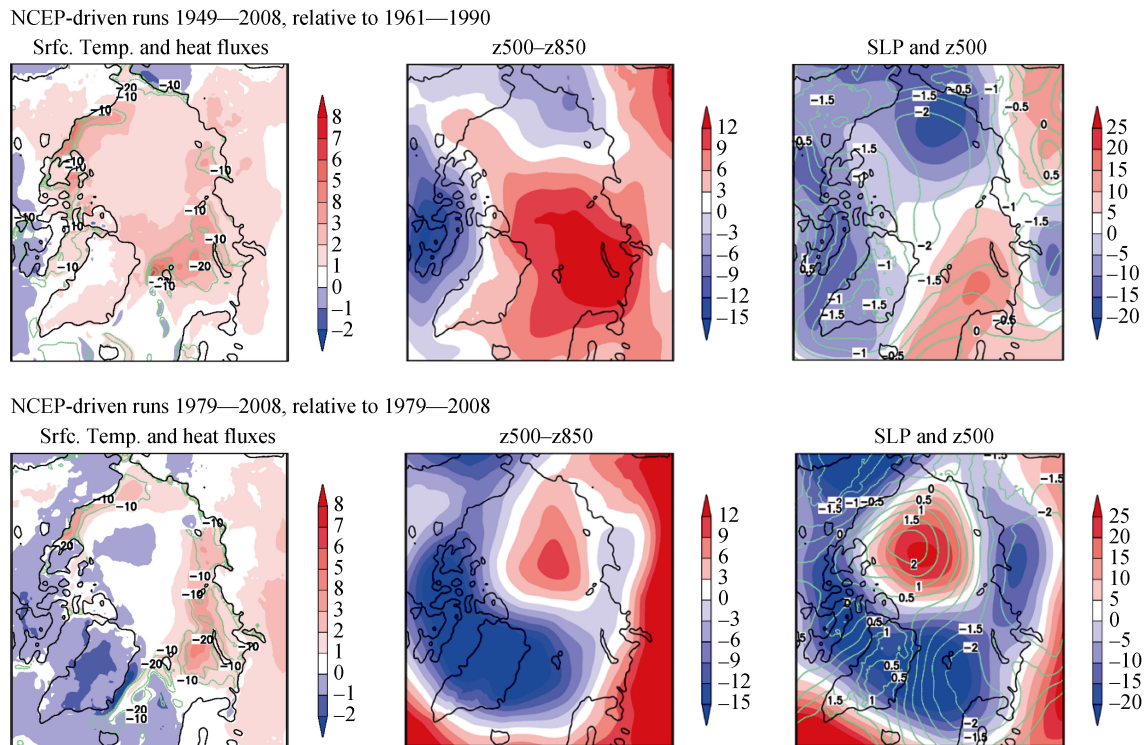


Figure 3 Simulated atmosphere differences “low minus high ice” for autumn, averaged over the respective ensemble members of the NCEP-driven runs. Left: surface air temperature (K; color shading) and sum of sensible and latent heat fluxes ($\text{W}\cdot\text{m}^{-2}$; negative: upward; green isolines); middle: geopotential thickness (m; z500–z850); right: mean sea level pressure (hPa; SLP; green isolines) and 500 hPa geopotential height (m; z500; color shading). The upper panel shows the results based on the full period 1949–2008 of the NCEP-driven runs and the low and high ice years have been selected with respect to the 1961–1990 mean. The lower panel shows the results based on the sub-period 1979–2008 of the NCEP-driven runs and the low and high ice years have been selected with respect to the 1979–2008 mean.

The differences of the 850–500 hPa thickness anomalies between the different composites are a consequence of interplays between sea-ice reduction, induced local thermodynamic forcing and changes in the atmospheric circulation (Figures 3 and 4). Positive/negative anomalies in the thickness of the free troposphere are associated with positive/negative anomalies of the 500 hPa geopotential height (z500), as z500 depends on the mean free-tropospheric temperature. Furthermore, z500 and the interdependent mean sea level pressure (SLP) serve as indicators of synoptic circulation changes. The “low minus high ice” z500 patterns do not show any similarity to each other (pattern correlation coefficients (*pcc*) range between

–0.10 and 0.38; see Table 1). An exception is the close similarity of the two patterns from the ERA-driven runs (*pcc*=0.97). Further, the atmospheric circulation anomalies in both long periods composites (NCEP-driven run 1949–2008 and ERA-driven run 1979–2014) share their baroclinic nature, associated with different patterns of pressure anomalies at the surface and in the mid-troposphere. Differently, the circulation anomalies from the composites over the 1979–2008 period (both from NCEP- and ERA-driven runs) are of rather equivalent barotropic structure. Table 1 summarizes the dissimilarity of the atmospheric circulation anomalies (exemplarily for z500) across the results.

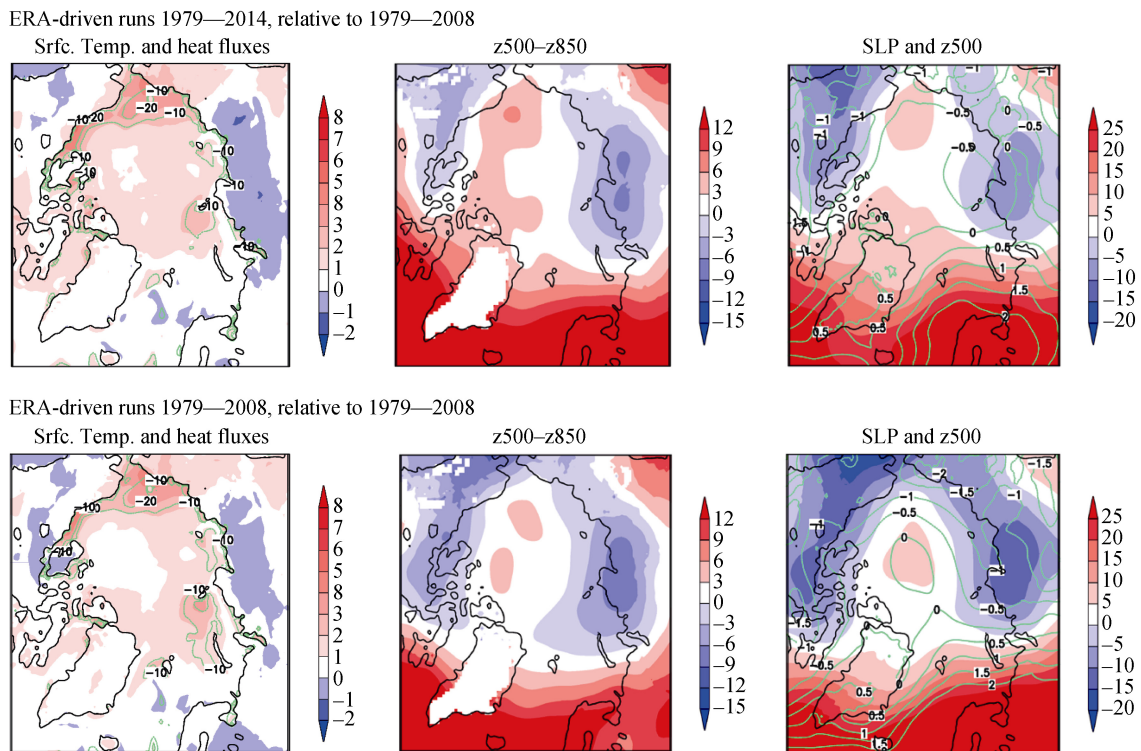


Figure 4 Simulated atmosphere differences “low minus high ice” for autumn, averaged over the respective ensemble members of the ERA-driven runs. Left: surface air temperature (K; color shading) and sum of sensible and latent heat fluxes ($\text{W}\cdot\text{m}^{-2}$; negative: upward; green isolines); middle: geopotential thickness (m; z500–z850); right: mean sea level pressure (hPa; SLP; green isolines) and 500 hPa geopotential height (m; z500; color shading). The upper panel shows the results based on the full period 1979–2014 of the ERA-driven runs. The lower panel shows the results based on the sub-period 1979–2008 of the ERA-driven runs. The low and high ice years have been selected in both with respect to the 1979–2008 mean.

Table 1 Pattern correlation coefficient of the simulated 500 hPa geopotential height “low minus high ice” anomaly patterns between each two pairs of the different runs (NCEP- or ERA-driven) and different periods for autumn (upper triangle) and winter (lower triangle; bold)

	NCEP-run 1949–2008	NCEP-run 1979–2008	ERA-run 1979–2008	ERA-run 1979–2014
NCEP-run 1949–2008	1	–0.10	0.38	0.35
NCEP-run 1979–2008	0.65	1	0.38	0.27
ERA-run 1979–2008	0.53	0.60	1	0.97
ERA-run 1979–2014	0.68	0.55	0.92	1

Comparing the “low minus high ice” circulation anomalies from the two periods of the NCEP-driven runs, it is obvious that they are distinctly different, likely as a result of the remarkably different heat fluxes and temperature anomalies. The circulation anomaly is even reversed over the Arctic Ocean. This means a negative pressure anomaly in the analysis based on 1949–2008, but a positive pressure anomaly in the analysis of 1979–2008. This difference may reflect a multi-decadal change in the atmospheric circulation in the context of Arctic sea-ice changes,

consistent with previous findings as represented by the Arctic Oscillation (AO) and the strength of the Beaufort high. AO has demonstrated a positive polarity until the early 1990s (Thompson and Wallace, 1998), suggesting a negative trend of SLP. Nevertheless, the Beaufort high has exhibited a strengthening trend during the recent decades (Wu et al., 2014), which is highly consistent with the SLP anomalies in Figure 3 (last panel). Differently, the comparison of the results from the two periods of the ERA-driven runs indicates quite similar atmospheric anomalies. This may suggest persistent features of sea-ice impacts during the recent decades even if the most recent low-ice years from 2009–2014 are included in the analysis. These features are characterized by large, opposite SLP anomalies between the North Atlantic-Europe sub-polar areas and the rest part of the sub-polar areas. This different imprint of the early and recent low-ice years on the atmospheric feedback appears although both sea-ice area anomalies are similarly strong (20%–30%) (Figure 1) and the sea-ice concentration anomalies of each of the two periods (from the NCEP-driven runs as well as from the ERA-driven runs) are similar and do not largely differ (Figure 2). One might speculate that different ocean conditions and/or atmospheric circulation patterns during the 1950s–1970s could play a role.

The comparison of the NCEP- and ERA-driven runs for the overlapping period 1979–2008 (Figures 3 and 4) highlights interesting regional differences in the temperature and circulation anomalies. On the one hand, their “low minus high ice” SLP and z500 patterns agree on a positive pressure anomaly over the Arctic Ocean (although much stronger in the NCEP-driven runs than in the ERA-driven runs) and a negative pressure anomaly over the surrounding land (Alaska, Siberia). In contrast, both runs indicate a largely different response over the Atlantic side of the Arctic. While the NCEP-driven runs show a negative pressure anomaly over the northern North Atlantic and the Barents/Kara Seas, the ERA-driven runs show a positive pressure anomaly. This different behavior across the Arctic occurs regardless of similar sea-ice forced heat flux anomalies over the Atlantic and Pacific sides of the Arctic in both runs, and seems to be related to the differences in the ‘background’ near surface temperature anomalies and associated tropospheric warming.

3.2 Winter

As in autumn, the “low minus high ice” anomalies in turbulent heat fluxes and SAT (Figure 5, Figure 6) show well-defined maxima, which are co-located with the sea-ice concentration anomaly in the Barents Sea (Figure 2). Due to the large

wintertime temperature difference between the cold atmosphere and the warm ocean, the anomalies in the sensible and latent heat fluxes are larger than in autumn and can reach up to $-140 \text{ W}\cdot\text{m}^{-2}$, with related local surface warming of up to 8 K. The similarity of the free-atmosphere anomalies across the results from the different runs and periods is striking though differences in the intensity of the anomalies exist.

Regardless of the different preceding autumn atmospheric anomalies, the results of the two periods from the NCEP-driven runs show rather similar atmospheric feedbacks in the subsequent winter (Figure 5). Both large-scale circulation anomalies reasonably agree ($pcc=0.65$ for z500; Table 1). An even stronger agreement of the atmospheric response occurs in the results of the two periods from the ERA-driven runs (Figure 6). The “low minus high ice” z500 anomalies are almost identical ($pcc=0.92$). Indeed, all results from both the NCEP- and ERA-driven runs agree on a quite similar atmospheric circulation feedback in winter, which is of equivalent barotropic structure from the surface to the troposphere as discussed by Rinke et al. (2013). The simulated free-atmosphere response does not depend on the selected runs or the periods and can be classified as robust. Table 1 summarizes the similarity of the atmospheric circulation anomalies (exemplarily for z500 in terms of pcc).

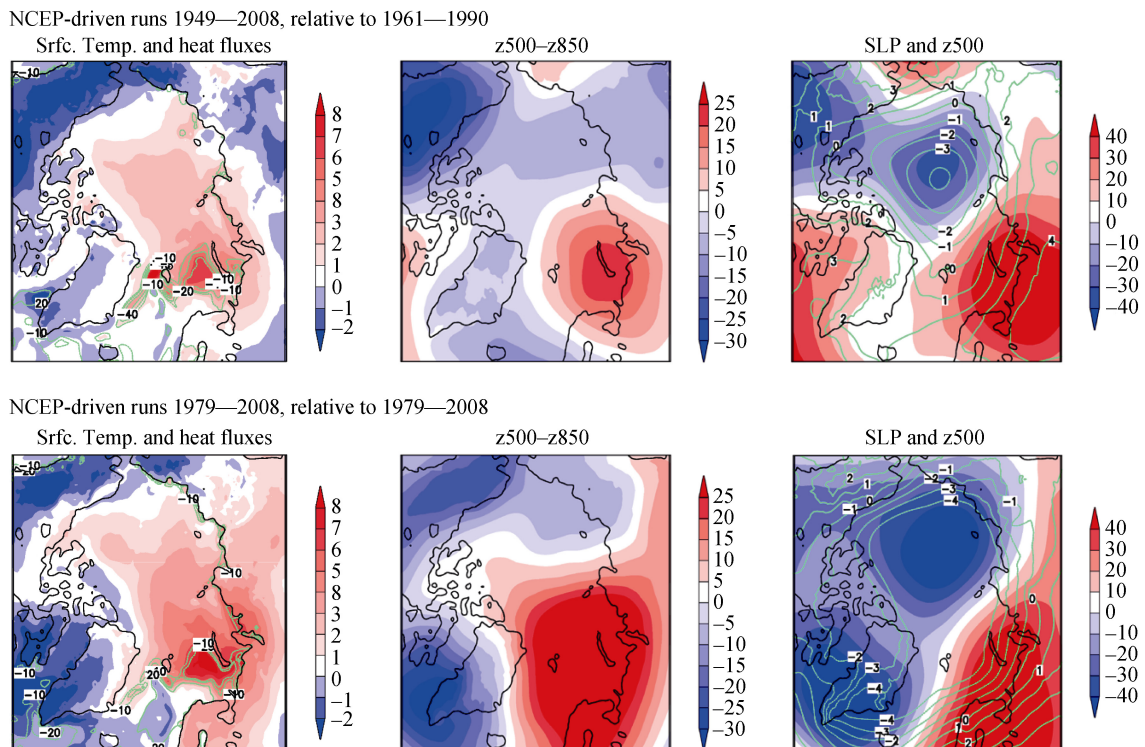


Figure 5 Simulated atmosphere differences “low minus high ice” for winter, averaged over the respective ensemble members of the NCEP-driven runs. Left: surface air temperature (K; color shading) and sum of sensible and latent heat fluxes ($\text{W}\cdot\text{m}^{-2}$; negative: upward; green isolines); middle: geopotential thickness (m; z500–z850); right: mean sea level pressure (hPa; SLP; green isolines) and 500 hPa geopotential height (m; z500; color shading). The upper panel shows the results based on the full period 1949–2008 of the NCEP-driven runs and the low and high ice years have been selected with respect to the 1961–1990 mean. The lower panel shows the results based on the sub-period 1979–2008 of the NCEP-driven runs and the low and high ice years have been selected with respect to the 1979–2008 mean.

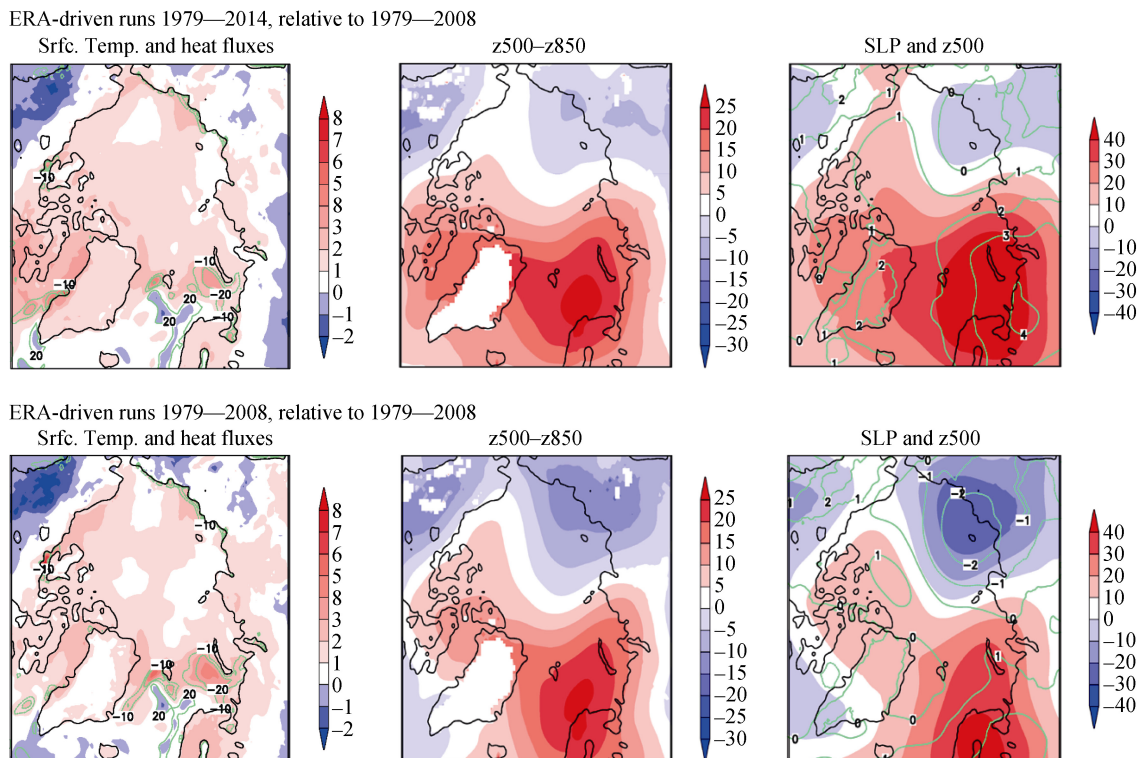


Figure 6 Simulated atmosphere differences “low minus high ice” for winter, averaged over the respective ensemble members of the ERA-driven runs. Left: surface air temperature (K; color shading) and sum of sensible and latent heat fluxes ($\text{W}\cdot\text{m}^{-2}$; negative: upward; green isolines); middle: geopotential thickness (m; z500–z850); right: mean sea level pressure (hPa; SLP; green isolines) and 500 hPa geopotential height (m; z500; color shading). The upper panel shows the results based on the full period 1979–2014 of the ERA-driven runs. The lower panel shows the results based on the sub-period 1979–2008 of the ERA-driven runs. The low and high ice years have been selected in both with respect to the 1979–2008 mean.

The simulated anomaly patterns are predominantly characterized by positive anomalies in the free-tropospheric thickness and pressure (z500 and SLP) over the Eurasian coastal lands and shelf seas with the maximum values centered in the region of the Barents/Kara Seas/Scandinavia/western Russia region. This has been related by earlier studies to a weakening of the North Atlantic storm track that branches towards the Barents/Kara Seas (e.g., Rinke et al., 2013; Inoue et al., 2012; Zhang et al., 2012). Negative anomalies occur over the East Siberian/Laptev Seas in the ERA-driven runs. In particular, comparison of the results during the two periods from the ERA-driven runs (Figure 6) indicates that the atmospheric “low minus high ice” anomalies in the Barents/Kara Seas region are stronger for the 1979–2014 period than for the shorter 1979–2008 period, which does not include the recent years of accelerated sea-ice decline. This SLP anomaly pattern and its change with time are consistent with previous observational findings. An emergence and intensification of anomalous high SLP over Eurasian coastal lands was detected since the beginning of this century when rapid winter sea-ice retreat, especially in the Barents and Kara Seas, occurred (Zhang et al., 2008). Recent studies (Crasemann et al., 2017; Gong and Luo 2017), which analyzed preferred circulation patterns in the North-Atlantic-Eurasian region, find a more frequent occurrence of a Scandinavian-Ural blocking

high for low Arctic sea-ice conditions in mid-winter (December and January).

4 Summary and conclusions

Different heat flux anomalies associated with the specific strength and position of the September sea-ice anomaly force distinctly different atmospheric feedbacks during autumn. Thus, the simulated atmospheric circulation response to low sea-ice conditions in autumn is sensitive to the considered period and to the setup of model simulations.

Regardless of the preceding autumn heat flux anomalies and atmospheric responses, a common free-atmosphere feedback in the following winter is established. This feedback is insensitive to the considered period and to the simulation setup.

The winter atmospheric change becomes particularly clear as a positive pressure anomaly over the Barents/Kara Seas (BKS) and Scandinavia/western Russia region. This positive pressure anomaly extends throughout the troposphere and the pattern can be interpreted as a manifestation of the so-called Scandinavian/Ural blocking. Its occurrence has been discussed as a dynamical response to anomalous surface heat sources as a consequence of winter sea-ice anomalies in the BKS. The basic

mechanism includes sea-ice forced diabatic processes (e.g., Dethloff et al., 2018; Luo et al., 2017; Jaiser et al., 2012; Petoukhov and Semenov, 2010; Honda et al., 2009). Anomalous turbulent heat fluxes and associated low-tropospheric heating lead to reduced atmospheric vertical static stability. This can increase the baroclinicity and thus amplify synoptic weather systems in the Arctic. The associated transient eddy forcing can excite large-scale planetary waves and impact the onset and maintenance of blockings downstream of areas with significant sea-ice retreat. In more detail, Inoue et al. (2012) found that a northward shift of cyclone paths during low sea-ice conditions over the BKS can create an anticyclonic circulation over the Scandinavian/Ural blocking region. Further, the warming over the BKS associated with the sea-ice retreat is associated with a reduced meridional temperature gradient, zonal winds and vertical wind shear over Eurasia and corresponds to an increased persistence of the Ural Blocking pattern (Luo et al., 2017).

The winter positive pressure anomaly with its center in the region of the BKS and Scandinavia/western Russia intensifies when recent years are included in the analysis of the ERA-driven runs. The emergence and intensification of this Scandinavian/Ural blocking were noticed in observations when rapid winter sea-ice retreat had already occurred, since the beginning of this century (Zhang et al., 2008). This is consistent with accelerated sea-ice retreat in the BKS in recent decades dynamically influencing the atmospheric circulation as discussed above. Importantly, only the sea-ice anomaly in the BKS persists from autumn to winter. The specification of the contribution from the autumn and winter sea-ice anomaly to the winter atmospheric circulation change is still an area of research. However, the comparison of the atmospheric feedbacks to regionally different sea-ice anomalies has shown, that the largest atmospheric response is driven by sea-ice anomalies in the BKS (Screen, 2017; Rinke et al., 2013).

The analyzed ensemble simulations are so-called free runs; no nudging has been applied. Nevertheless, the atmospheric ‘background’ circulation, given by the NCEP/NCAR or ERA-Interim atmospheric lateral boundaries, potentially affects the simulated atmospheric response. The quantification of its contribution to the differences in the simulated atmospheric feedbacks will be a next step in our research.

Acknowledgments This study has been supported by the SFB/TR172 “Arctic Amplification: Climate Relevant Atmospheric and Surface Processes, and Feedback Mechanisms (AC)” funded by the Deutsche Forschungsgemeinschaft (DFG). This work has been further supported by the project QUARCCS “Quantifying Rapid Climate Change in the Arctic: Regional feedbacks and large-scale impacts” funded by the German Federal Ministry for Education and Research (BMBF). The authors thank two anonymous reviewers for their evaluation and helpful comments.

References

- Cohen J, Screen J A, Furtado J C, et al. 2014. Recent Arctic amplification and extreme mid-latitude weather. *Nature Geosci*, 7: 627-637, doi:10.1038/ngeo2234.
- Crasemann B, Handorf D, Jaiser R, et al. 2017. Can preferred atmospheric circulation patterns over the North-Atlantic-Eurasian region be associated with Arctic sea ice loss? *Polar Science*, 14: 9-20, doi:10.1016/j.polar.2017.09.002.
- Dee D P, Uppala S M, Simmons A J, et al. 2011. The ERA-Interim reanalysis: Configuration and performance of the data assimilation system. *Q J Roy Meteor Soc*, 137(656): 553-597, doi:10.1002/qj.828.
- Dethloff K, Handorf D, Jaiser R, et al. 2018. Dynamical mechanisms of Arctic amplification. *Ann N Y Acad Sci*, doi:10.1111/nyas.13698.
- Dorn W, Dethloff K, Rinke A. 2009. Improved simulation of feedbacks between atmosphere and sea ice over the Arctic Ocean in a coupled regional climate model. *Ocean Modelling*, 29(2): 103-114, doi:10.1016/j.ocemod.2009.03.010.
- Dorn W, Dethloff K, Rinke A. 2012. Limitations of a coupled regional climate model in the reproduction of the observed Arctic sea-ice retreat. *The Cryosphere*, 6: 985-998, doi:10.5194/tc-6-985-2012.
- Gong T, Luo D. 2017. Ural blocking as an amplifier of the Arctic sea ice decline in winter. *J Clim*, 30: 2639-2654, doi:10.1175/JCLI-D-16-0548.1.
- Honda M, Inoue J, Yamane S. 2009. Influence of low Arctic sea - ice minima on wintertime Eurasian coldness. *Geophys Res Lett*, 36: L08707, doi:10.1029/2008GL037079.
- Inoue J, Hori M E, Takaya K. 2012. The role of Barents Sea ice in the wintertime cyclone track and emergence of a warm-Arctic cold-Siberian anomaly. *J Clim*, 25(7): 2561-2568, doi:10.1175/JCLI-D-11-00449.1.
- Jaiser R, Dethloff K, Handorf D, et al. 2012. Impact of sea ice cover changes on the Northern Hemisphere atmospheric winter circulation. *Tellus A*, 64: 11595, doi:10.3402/tellusa.v64i0.11595.
- Jaiser R, Nakamura T, Handorf D, et al. 2016. Atmospheric winter response to Arctic sea ice changes in reanalysis data and model simulations. *J Geophys Res*, 121: 7564-7577, doi:10.1002/2015-JD024679.
- Jeffries M O, Overland J E, Perovich D K. 2013. The Arctic shifts to a new normal. *Physics Today*, 66 (10): 35-40, doi:10.1063/PT.3.2147.
- Kalnay E, Kanamitsu M, Kistler R, et al. 1996. The NCEP/NCAR 40-year reanalysis project. *Bull Am Meteorol Soc*, 77(3): 437-471.
- Luo D, Yao Y, Dai A, et al. 2017. Increased quasi stationarity and persistence of winter Ural blocking and Eurasian extreme cold Events in response to arctic warming. Part II: A theoretical explanation. *J Clim*, 30(10): 3569-3587, doi:10.1175/JCLI-D-16-0262.1.
- Peings Y, Magnusdottir G. 2014. Response of the Wintertime Northern Hemisphere Atmospheric Circulation to Current and Projected Arctic Sea Ice Decline: A Numerical Study with CAM5. *J Clim*, 27: 244-264, doi:10.1175/JCLI-D-13-00272.1.
- Petoukhov V, Semenov V A. 2010. A link between reduced Barents - Kara sea ice and cold winter extremes over northern continents. *J Geophys Res*, 115: D21111, doi:10.1029/2009JD013568.
- Porter D F, Cassano J J, Serreze M C. 2012. Local and large-scale atmospheric responses to reduced Arctic sea ice and ocean warming in the WRF model. *J Geophys Res*, 117: D11115, doi:10.1029/2011JD016969.

- Rinke A, Dethloff K, Dorn W, et al. 2013. Simulated Arctic atmospheric feedbacks associated with late summer sea ice anomalies. *J Geophys Res Atmos*, 118: 7698-7714, doi:10.1002/jgrd.50584.
- Rinke A, Maslowski W, Dethloff K, et al. 2006. Influence of sea ice on the atmosphere: A study with an Arctic atmospheric regional climate model. *J Geophys Res*, 111: D16103, doi:10.1029/2005JD006957.
- Screen J, Deser C, Simmonds I, et al. 2013. The atmospheric response to three decades of observed Arctic sea ice loss. *J Clim*, 26: 1230-1248, doi:10.1175/JCLI-D-12-00063.1.
- Screen J A. 2017. Simulated atmospheric response to regional and Pan-Arctic sea-ice loss. *J Clim*, 30: 3945-3962, doi:10.1175/JCLI-D-16-0197.1.
- Semenov V A, Latif M. 2015. Nonlinear winter atmospheric circulation response to Arctic sea ice concentration anomalies for different periods during 1966–2012. *Environ Res Lett*, 10(5): 054020, doi:10.1088/1748-9326/10/5/054020.
- Serreze M C, Barry R G. 2011. Processes and impacts of Arctic amplification: A research synthesis. *Glob Planet Change*, 77(1-2): 85-96, doi:10.1016/j.gloplacha.2011.03.004.
- Stroeve J C, Serreze M C, Kay J E, et al. 2012. The Arctic's rapidly shrinking sea ice cover: A research synthesis. *Clim Change*, 110: 1005-1027, doi:10.1007/s10584-011-0101-1.
- Thompson D W J, Wallace J M. 1998. The Arctic Oscillation signature in the wintertime geopotential height and temperature fields. *Geophys Res Lett*, 25: 1297-1300.
- Vihma T. 2014. Effects of Arctic sea ice decline on weather and climate: a review. *Surv Geophys*, 35: 1175, doi:10.1007/s10712-014-9284-0.
- Wendisch M, Brückner M, Burrows J P, et al. 2017. Understanding causes and effects of rapid warming in the Arctic. *EOS*, 98, doi:10.1029/2017EO064803.
- Wu Q, Zhang J, Zhang X, et al. 2014. Interannual Variability and Long-Term Changes of Atmospheric Circulation over the Chukchi and Beaufort Seas. *J Clim*, 27: 4871-4889, doi:10.1175/JCLI-D-13-00610.1.
- Zhang X, Lu C, Guan Z. 2012. Weakened cyclones, intensified anticyclones and recent extreme cold winter weather events in Eurasia. *Environ Res Lett*, 7: 044044, doi:10.1088/1748-9326/7/4/044044.
- Zhang X, Sorteberg A, Zhang J, et al. 2008. Recent radical shifts in atmospheric circulations and rapid changes in Arctic climate system. *Geophys Res Lett*, 35: L22701, doi:10.1029/2008GL035607.